DALTON
FULL PAPER

The solution structure of supramolecular lanthanide triple helices revisited: application of crystal-field independent paramagnetic NMR techniques to mono- and di-metallic complexes†

Stéphane Rigault,[a] Claude Piguet[a] and Jean-Claude G. Bünzli[b]

[a] *Department of Inorganic, Analytical and Applied Chemistry, University of Geneva, 30 quai E. Ansermet, CH-1211 Geneva 4, Switzerland. E-mail: Claude.Piguet@chiam.unige.ch*
[b] *Institute of Inorganic and Analytical Chemistry, University of Lausanne, BCH 1402, CH-1015 Lausanne, Switzerland*

Received 10th January 2000, Accepted 25th April 2000
Published on the Web 6th June 2000

Pyridine-containing tridentate binding units react with trivalent lanthanide ions, Ln^{III}, to give C_3-symmetrical nine-coordinate triple helical complexes in which subtle intramolecular interactions control the final structures. While X-ray crystal structures allow some rationalisation in the solid state, the access to solution structures by paramagnetic NMR is limited by the unpredictable variation of the crystal-field parameter along the lanthanide series. A recent technique which considers two different nuclei within the same complex overcomes this drawback and its application to triple helical lanthanide complexes of increasing sophistication is described. This new approach confirms the previously suggested geometrical change occurring in the monometallic complexes $[Ln(L^2)_3]^{3+}$ for the heavier lanthanides. Its use in the case of the heterodimetallic triple-stranded helicates $[LnCo(L^4)_3]^{6+}$ evidences a single isostructural series while the separation of contact and pseudo-contact contributions according to classical techniques gives intractable results. Finally, new equations are derived for homodimetallic complexes with large Ln···Ln separation and they are applied to the structural analysis of the triple-stranded helicates $[Ln_2(L^5 - 2H)_3]$. The latter reveals that the dimetallic edifices display a single solution structure along the complete lanthanide series in contrast with a previous analysis considering invariant crystal-field parameters. The scope and limitations of this technique for supramolecular lanthanide complexes is discussed together with specific effects resulting in amplification of magnetic properties in polymetallic systems.

Introduction

Our recent attempts to control the geometry and structure of the coordination spheres in lanthanide complexes according to the *induced fit* concept rely on subtle structural constraints associated with non-covalent interactions occurring in the final supramolecular architecture.[1] Semi-rigid bent tridentate binding units are particularly well-suited for this purpose since the helical wrapping of three strands about the metal provides a nine-coordinate pseudo-tricapped trigonal prismatic coordination site suitable for the complexation of trivalent lanthanides, Ln^{III}.[1] Although 2,2′:6′2″ terpyridine, the archetype of a semi-rigid bent tridentate binding unit, gives poorly stable 1:3 triple helical complexes $[Ln(terpy)_3]^{3+}$ in solution,[2] the replacement of the pyridine side arms by oxygen donors (L^1, L^2) or extended heterocyclic groups (L^3) significantly (i) improves the stability of the final triple-helical complexes $[Ln(L^1 - 2H)_3]^{3-}$[3] and $[Ln(L^i)_3]^{3+}$ ($i = 2, 3$)[4,5] and (ii) implements subtle non-covalent intramolecular interactions which can modulate size-discriminating effects and molecular structures.

Electrostatic repulsion between terminal carboxylate groups in $[Ln(L^1 - 2H)_3]^{3-}$ is responsible for the lower stability with small Ln^{III} ions,[1,3] intramolecular steric constraints induce structural variations along the lanthanide series for $[Ln(L^2)_3]^{3+}$,[4] while interstrand π-stacking interactions have been invoked for explaining the unprecedented selectivity of $[Ln(L^3)_3]^{3+}$ for mid-range Ln^{III}.[5] However, an accurate description of the molecular structures for these complexes systematically relies on X-ray crystal structures which reflect solid-state behaviour, while the programmed subtle selectivity associated with intramolecular steric constraints depend on solution structures which are difficult to address with classical techniques.[1,5]

The recent design of extended metallosupramolecular edifices from hetero-[6,7] and homo-polymetallic[8,9] lanthanide-containing complexes suffers from this duality which limits the characterisation of the final supramolecular structures in solution and consequently the rationalisation of the assembly processes leading to their formation. Paramagnetic NMR has been recognised as an efficient tool for elucidating the solution structures of paramagnetic lanthanide complexes, particularly for axial complexes (*i.e.* possessing at least a threefold axis)[10] displaying close geometrical structures along the lanthanide series (*i.e.* considered as an isostructural series).[11–13] The application of the structure-independent technique of Reilley and co-workers[13] for the dissection of contact and pseudo-contact contributions to the paramagnetic NMR shifts in $[Ln(L^1 - 2H)_3]^{3-}$ revealed a single D_3-symmetrical structure in solution along the complete lanthanide series which contrasts with the small, but significant, structural variations observed in the solid state between large and small Ln^{III} ions.[3] The limited accuracy of the separation of contact and pseudo-contact contributions prevents the detection of minor structural changes, but the same procedure applied to $[Ln(L^2)_3]^{3+}$ reveals a break between Tb and Er which has been assigned to different arrangements of the ligand strands in the final complexes.[4]

The situation is less clear for extended dimetallic supramolecular complexes and accurate solution structures for the triple-helical complexes $[LnZn(L^4)_3]^{5+}$ (Ln = Ce–Yb) cannot be

† Electronic supplementary information (ESI) available: geometric ratios. See http://www.rsc.org/suppdata/dt/b0/b000147n/

DOI: 10.1039/b000147n

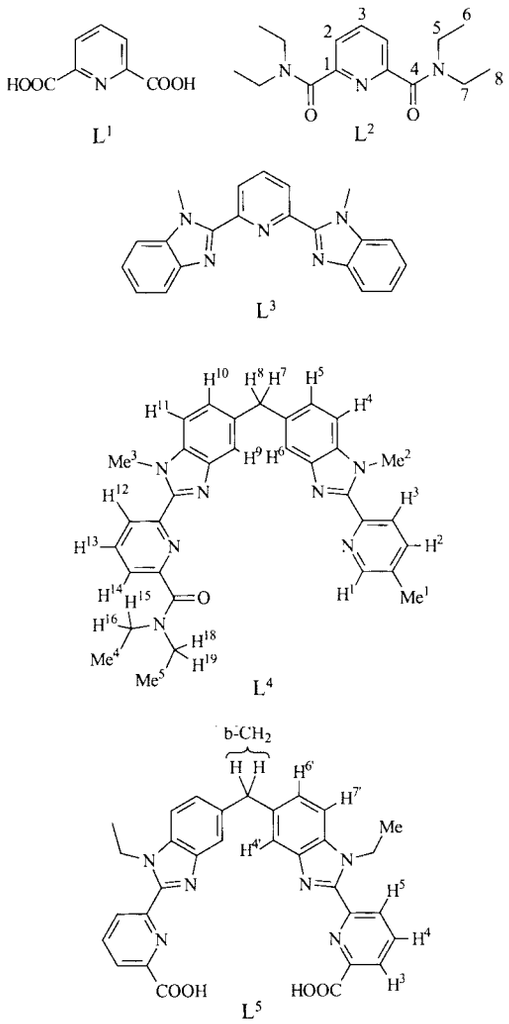

obtained[6] although the experimental axial magnetic susceptibility tensors have been determined according to the method of Kemple and co-workers.[14] The recent extension of these techniques to homodimetallic lanthanide complexes[9] demonstrates that the triple-stranded helicates $[Ln_2(L^5 - 2H)_3]$ also exhibit a break between Tb and Er, but its assignment to a sizable geometrical change and/or to variation in the crystal-field parameter is not straightforward. Moreover, simulations of the classical contraction of the ionic radii in axial lanthanide complexes by using molecular mechanics[12] or variations of the crystal-field parameter for small Ln^{III} [15,16] predict the appearance of 'artificial' breaks around the middle of the lanthanide series which are not diagnostic of any major structural changes. This classical approach reaches its limit in $[LnCo(L^4)_3]^{6+}$ for which the ^{1}H-NMR spectra with small Ln^{III} (Ln = Ho–Yb) cannot be explained.[7] In this paper, we re-examine the solution structures of C_3-symmetrical triple-helical complexes $[Ln(L^2)_3]^{3+}$, $[LnCo(L^4)_3]^{6+}$ and $[Ln_2(L^5 - 2H)_3]$ displaying increasing structural complexities by using a new crystal-field parameter independent method first introduced by Reuben for monometallic shift reagents[16] and recently adapted by Geraldes and co-workers for lanthanide cryptates.[17]

Theory

The NMR shift δ_{ij} induced at a nucleus i of a ligand bound to a lanthanide j can be expressed as the sum of the diamagnetic shift δ_i^{dia} (given by the NMR shift of the related complexes with Ln = La, Y or Lu), the paramagnetic contact shift δ_{ij}^{c} (associated with through-bond Fermi interactions),[18] the paramagnetic pseudo-contact shift δ_{ij}^{pc} (associated with the residual through-space dipolar interaction)[19] and the shift due to the bulk magnetic susceptibility of the sample δ_j^{bulk} [eqn. (1)].[20] The

$$\delta_{ij} = \delta_i^{dia} + \delta_{ij}^{c} + \delta_{ij}^{pc} + \delta_j^{bulk} \quad (1)$$

latter contribution (δ_j^{bulk}) can be estimated from the magnetic moment of the dissolved paramagnetic complex,[21] but it affects similarly all nuclei and therefore cancels out when chemical shifts are referenced to an internal standard.[5] The isotropic paramagnetic shift for a nucleus i in the complex of a lanthanide j, Δ_{ij}, is thus given by eqn. (2) in which the contact and

$$\Delta_{ij} = \delta_{ij} - \delta_i^{dia} = \delta_{ij}^{c} + \delta_{ij}^{pc} = F_i \cdot \langle S_z \rangle_j + G_i \cdot \{A_2^0 \cdot \langle r^2 \rangle\} \cdot \frac{C_j}{T^2} \quad (2)$$

pseudo-contact terms have been developed according to well-established theories.[22]

$\langle S_z \rangle_j$ is the projection of the total electron spin magnetisation of the lanthanide j onto the direction of the external magnetic field, C_j is a magnetic constant at a given temperature T measuring the second-order magnetic axial anisotropy of the paramagnetic lanthanide j (Bleaney factor)[19] and $\{A_2^0 \cdot \langle r^2 \rangle\}$ is the crystal-field parameter which measures the magnitude of the interaction between a given lanthanide j and the ligand donor atoms. These three terms essentially depend on the lanthanide j in a homogeneous series of complexes and the tabulated free-ion values of $\langle S_z \rangle_j$[18] and C_j[19] can be used as good approximations of their relative experimental values in axial lanthanide complexes.[22] F_i corresponds to the product of the electron-nuclear hyperfine coupling constant with a temperature-dependent coefficient and it thus only depends on the nucleus i and on its topological location in the complex. Finally, G_i is the geometric factor of nucleus i that contains the structural information about the complex [eqn. (3)] where θ_i is the angle

$$G_i = \frac{1 - 3\cos^2\theta_i}{r_i^3} \quad (3)$$

between the Ln–(nucleus i) vector and the main axis (z-axis) of the magnetic susceptibility tensor of the complex (*i.e.* the main molecular symmetry axis in axial complexes with at least a threefold symmetry)[10] and r_i is the Ln–(nucleus i) distance (Fig. 1).

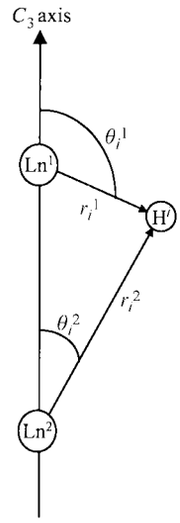

Fig. 1

Eqn. (2) is ideally suited for a straightforward multi-linear least-squares separation of contact (F_i) and pseudo-contact (G_i) terms at a fixed temperature in an isostructural series of at least two-different axial paramagnetic lanthanide complexes if three hypotheses are fulfilled: (1) the free-ion values of $\langle S_z \rangle_j$ and C_j are similar to those found in the complexes, (2) F_i is invariant for the complexes along the lanthanide series and (3) the

crystal-field parameter $\{A_2^0 \cdot \langle r^2 \rangle\}$ is constant along the series. The validity of the first two assumptions has been convincingly established,[18,23] but the last hypothesis is doubtful despite its general acceptance and a recent investigation concludes to its failure for C_4-symmetrical macrocyclic complexes.[15] Nevertheless, the rearrangement of eqn. (2) leads to two linear forms for which we expect linear plots of $\Delta_{ij}/\langle S_z \rangle_j$ *vs.* $C_j/\langle S_z \rangle_j$ [eqn. (4)]

$$\frac{\Delta_{ij}}{\langle S_z \rangle_j} = F_i + \frac{G_i}{T^2} \cdot \{A_2^0 \cdot \langle r^2 \rangle\} \cdot \frac{C_j}{\langle S_z \rangle_j} \quad (4)$$

and Δ_{ij}/C_j *vs.* $\langle S_z \rangle_j/C_j$ [eqn. (5)] for each nucleus i within an

$$\frac{\Delta_{ij}}{C_j} = F_i \cdot \frac{\langle S_z \rangle_j}{C_j} + \frac{G_i}{T^2} \cdot \{A_2^0 \cdot \langle r^2 \rangle\} \quad (5)$$

isostructural series of complexes with lanthanide j when the above-mentioned hypotheses are satisfied.[22]

Any deviations of these plots from linearity along the lanthanide series are generally interpreted as structural changes which affect F_i and/or G_i[22] and the strict application of these criteria to triple-helical complexes led to the conclusion that two differently packed structures occur for $[Ln(L^2)_3]^{3+}$[4] and $[Ln_2(L^5 - 2H)_3]$,[9] while $[LnZn(L^4)_3]^{5+}$ display a single isostructural series from Ce to Yb.[8] However, it has been suggested that breaks in the linear plots defined by eqns. (4) and (5) are not necessarily associated with significant structural changes since the well-known lanthanide contraction[12] and/or minor variations of the crystal-field parameter[15,16] may induce such effects. In order to remove the effect of the crystal-field, Reuben[16] first introduced a shift modulation function which considers the simultaneous chemical shifts Δ_{ij} and Δ_{kj} of two nuclei i and k within the same ligand for various lanthanides j. The original function, which has been later applied to macrocyclic complexes,[15] used Yb as a reference,[16] but Geraldes and co-workers have extended this approach by simultaneously solving eqn. (2) for two different nuclei [eqns. (6) and (7)], which eventually leads to eqn. (8).[17]

$$\Delta_{ij} = F_i \cdot \langle S_z \rangle_j + G_i \cdot \{A_2^0 \cdot \langle r^2 \rangle\} \cdot \frac{C_j}{T^2} \quad (6)$$

$$\Delta_{kj} = F_k \cdot \langle S_z \rangle_j + G_k \cdot \{A_2^0 \cdot \langle r^2 \rangle\} \cdot \frac{C_j}{T^2} \quad (7)$$

$$\frac{\Delta_{ij}}{\langle S_z \rangle_j} = \left(F_i - F_k \cdot \frac{G_i}{G_k} \right) + \frac{G_i}{G_k} \cdot \frac{\Delta_{kj}}{\langle S_z \rangle_j} \quad (8)$$

$$R_{ik} = \frac{G_i}{G_k} = \frac{1 - 3\cos^2 \theta_i}{1 - 3\cos^2 \theta_k} \cdot \frac{r_k^3}{r_i^3} \quad (9)$$

Plots of $\Delta_{ij}/\langle S_z \rangle_j$ *vs.* $\Delta_{kj}/\langle S_z \rangle_j$ within an isostructural series are expected to be linear with a slope R_{ik} [eqn. (9)] and an intercept equal to $(F_i - F_k) \cdot R_{ik}$. Since variations of the crystal-field parameter do not affect eqn. (8), any deviation from linearity leading to different slopes can be safely interpreted as a geometrical change along the lanthanide series. Moreover, breaks observed along the lanthanide series according to eqns. (4) and (5) may also originate from variations of the hyperfine electron-nuclear constants which can be detected from different intercepts in eqn. (8).[17]

Results and discussion

Monometallic triple helical complexes: $[Ln(L^2)_3]^{3+}$

A detailed analysis of the isotropic paramagnetic NMR shifts of these complexes (Ln = Ce–Yb) in acetonitrile according to Reilley's method [eqns. (2), (4) and (5)] and variable temperature data have led to the following statements.[4] (1) The use of eqns. (4) and (5) for H[2,3,5–8] and C[1–8] systematically provides two straight lines involving respectively large (Ce–Tb) and small (Er–Yb) Ln^{III} ions thus pointing to different structures in solution (Fig. 2). (2) The $G_i \cdot \{A_2^0 \cdot \langle r^2 \rangle\}$ values extracted for H^i and C^i confirm this geometrical change between Tb and Er and strongly suggest a flattening of the triple helical structure along the C_3 axis for the small Ln^{III} ions. (3) A D_3-symmetrical triple-helical structure dynamically inert on the NMR time scale can be assigned to $[Ln(L^2)_3]^{3+}$ (Ln = Er–Yb), while fast interconversion between the helical enantiomers (P $\rightleftharpoons$ M) on the NMR time scale produces dynamically-averaged D_{3h}-symmetrical complexes for Ln = La–Tb at room temperature. (4) The X-ray crystal structures obtained for the La and Eu complexes reveal a C_2-symmetrical arrangement in $[Eu(L^2)_3]^{3+}$ close to a regular triple helix (Fig. 3), while $[La(L^2)_3]^{3+}$ evidences drastic distortions associated with a significant bending of the tridentate binding units.[4] We thus concluded[4] that the breaks in the linear plots [eqns. (4)–(5)] probably reflect significant changes in the G_i factors for these complexes along the lanthanide series, although no reliable trend could be deduced for the crystal-field parameter.

Plots of $\Delta_{ij}/\langle S_z \rangle_j$ *vs.* $\Delta_{kj}/\langle S_z \rangle_j$ for all possible pairs of nuclei H^i/H^k, C^i/C^k and H^i/C^k ($i \neq k$) according to eqn. (8) systematically

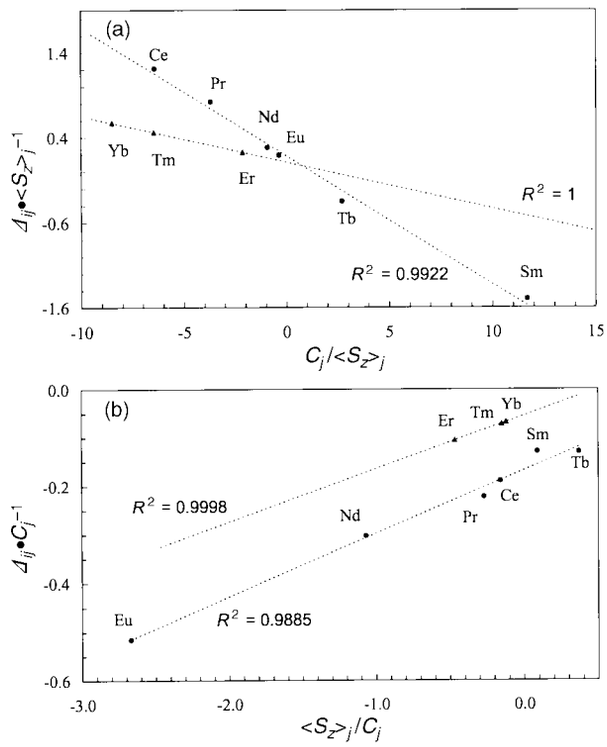

Fig. 2 Plots of (a) $\Delta_{ij} \cdot \langle S_z \rangle_j^{-1}$ *vs.* $C_j \cdot \langle S_z \rangle_j^{-1}$ [eqn. (4)] and (b) $\Delta_{ij} \cdot C_j^{-1}$ *vs.* $\langle S_z \rangle_j \cdot C_j^{-1}$ [eqn. (5)] for H^2 in $[Ln(L^2)_3]^{3+}$ (acetonitrile, 298 K, redrawn from ref. 4).

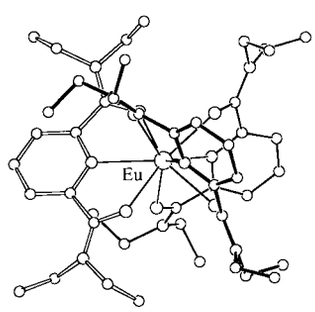

Fig. 3 ORTEP[24] view of $[Eu(L^2)_3]^{3+}$ perpendicular to the pseudo-C_3 axis in the crystal structure of $[Eu(L^2)_3](O_3SCF_3)_3$.[4]

Table 1 Minimal set of geometric ratio $R_{ik} = G_i \cdot G_k^{-1}$ obtained from plots of $\Delta_{ij} \cdot \langle S_z \rangle_j^{-1}$ *vs.* $\Delta_{kj} \cdot \langle S_z \rangle_j^{-1}$ according to eqn. (8) for $[Ln(L^2)_3]^{3+}$ (CD_3CN, 298 K)[a]

	H^2–H^3	H^2–C^1	H^2–C^2	H^2–C^3	H^2–C^4
R_{ik} (Ce–Tb)[b]	0.93(5)	0.33(3)	0.39(3)	0.91(4)	−0.7(3)
R_{ik} (Er–Yb)[c]	1.02(9)	0.14(8)	1.38(6)	0.65(4)	0.08(2)
R_{ik} ($[Eu(L^2)_3]^{3+}$)[d]	1.018	0.213	0.499	0.591	16.321

[a] A complete set of R_{ik} data generated according to $R_{ik} = R_{ij} \cdot R_{jk}$ is given in the supporting information together with the experimental and calculated intercepts $F_i - R_{ik} \cdot F_k$ (Table S1). [b] Values for the first isostructural series (Sm has been removed because of its faint paramagnetic induced shift).[4] [c] Values for the second isostructural series. [d] Calculated from the crystal structure of $[Eu(L^2)_3](CF_3SO_3)_3$ after averaging to D_3 symmetry.[4]

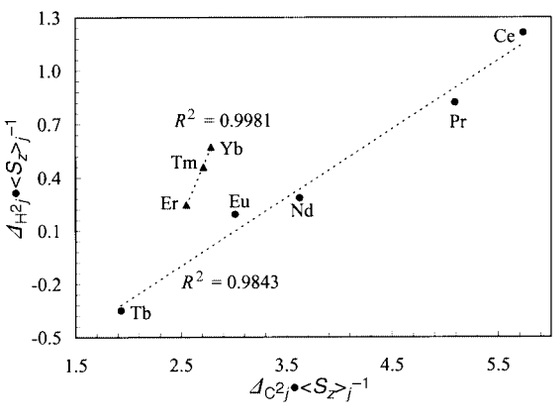

Fig. 4 Plot of $\Delta_{ij} \cdot \langle S_z \rangle_j^{-1}$ *vs.* $\Delta_{kj} \cdot \langle S_z \rangle_j^{-1}$ according to eqn. (8) for H^2–C^2 in $[Ln(L^2)_3]^{3+}$ (acetonitrile, 298 K).

show two different straight lines (Ln = Ce–Tb and Er–Yb respectively, Fig. 4) which unambiguously confirm that the original breaks observed according to eqns. (4) and (5) can be assigned to a geometrical change which occurs between Tb and Er. The experimental slopes $R_{ik} = G_i/G_k$ and intercepts $(F_i - F_k) \cdot R_{ik}$ for i, k = 1–4 are collected in Table 1 together with expected values calculated from the D_3-averaged X-ray crystal structure of $[Eu(L^2)_3](CF_3SO_3)_3$ and the F_i and F_k values extracted from eqn. (2).[4]

Data for i, k = 5–8 are not considered because the ethyl chains are flexible and their arrangement in the solid state strongly depends on packing forces which have no counterpart in solution. Moreover, the angular co-ordinate of C^4 (θ_{C^4} = 54.9°) in the crystal structure of $[Eu(L^2)_3]^{3+}$ is close to the magic angle (54.7°), which precludes reliable prediction for R_{ik} for the pairs involving this nuclei since $G_{C^4} \approx 0$. Indeed, Peters and co-workers[12] have previously reported that minor geometrical changes have a drastic effect on this term close to the magic angle and lead to large discrepancies when the solution structure is compared to a solid-state model. For the remaining pairs, the R_{ik} values found for both series are in qualitative agreement with those calculated from the crystal structure and a rough test of similarity between the crystal structure and the two solution structures can be obtained with the calculation of the Wilcott agreement factors [eqn. (10)][13] which amount to

$$AF_{slope} = \sqrt{\frac{\Sigma_{i,k}\,[R_{ik}^{exp} - R_{ik}^{calc}]^2}{\Sigma_{i,k}\,(R_{ik}^{exp})^2}}$$

$$AF_{intercept} = \sqrt{\frac{\Sigma_{i,k}\,[(F_i - F_k \cdot R_{ik}^{exp}) - (F_i - F_k \cdot R_{ik}^{calc})]^2}{\Sigma_{i,k}\,(F_i - F_k \cdot R_{ik}^{exp})^2}} \quad (10)$$

$AF_{slope} = 0.42$ (Ce–Tb) and $AF_{slope} = 0.61$ (Er–Yb) and $AF_{intercept} = 0.06$ (Ce–Tb) and $AF_{intercept} = 0.14$ (Er–Yb). Since the AF factors are significantly smaller for the first isostructural series, we conclude that the crystal structure of $[Eu(L^2)_3]^{3+}$ is a better model for the solution structure of $[Ln(L^2)_3]^{3+}$ with large lanthanide metal ions (Ce–Tb), while smaller Ln^{III} ions induce a more compact structure which is slightly flattened along the C_3-axis as previously established from the qualitative analysis of the $G_i \cdot \{A_2^0 \cdot \langle r^2 \rangle\}$ factors.[4]

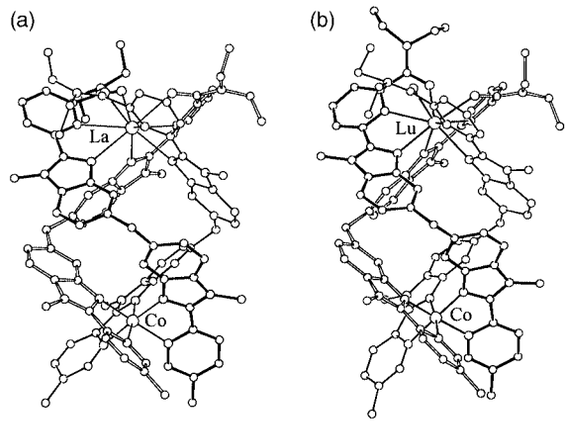

Fig. 5 ORTEP[24] views of (a) $[LaCo(L^4)_3]^{6+}$ and (b) $[LuCo(L^4)_3]^{6+}$ perpendicular to the pseudo-C_3 axis in the crystal structure of $[LaCo(L^4)_3](ClO_4)_{5.5}(OH)_{0.5}$[7] and $[LuCo(L^4)_3](O_3SCF_3)_6$.‡

The only limited match between the crystal structure of $[Eu(L^2)_3]^{3+}$ and its solution structure as measured by the large AF_{slope} factors is not unexpected because the fast dynamic interconversion between helical enantiomers observed on the NMR time scale in solution produces an average structure which differs significantly from that found in the solid state.

Heterodimetallic d–f triple helical complexes: $[LnCo(L^4)_3]^{6+}$

The extension of the helical ligand strand to incorporate two or more metal ions produces helicates[25] whose kinetic stability is significantly larger compared to monometallic precursors[26] and the assembly process of L^4 with cobalt and Ln^{III} produces kinetically inert head-to-head C_3-symmetrical heterotopic triple-stranded helicates (HHH)–$[LnCo(L^4)_3]^{6+}$.[7] In these complexes, the d-block ion occupies the pseudo-octahedral site defined by the three bidentate binding units of the segmental ligands and controls the arrangement of the strands for their facial co-ordination to Ln^{III}. The introduction of low-spin diamagnetic and kinetically inert Co^{III} in $[LnCo(L^4)_3]^{6+}$ is particularly suitable for the study of the solution behaviour of these complexes by paramagnetic NMR since Ln^{III} is the only paramagnetic centre in the supramolecular complex. The X-ray crystal structures of $[LaCo(L^4)_3]^{6+}$[7] and $[LuCo(L^4)_3]^{6+}$‡ unambiguously establish the formation of triple helices in which the three strands are wrapped around the metal ions which define a pseudo-C_3 axis (Fig. 5). The close similarity between these structures suggest that no major geometrical change occurs along the lanthanide series and the almost identical ^1H NMR spectra recorded for the diamagnetic complexes $[LnCo(L^4)_3]^{6+}$ (Ln = La, Y, Lu) in acetonitrile confirm the exclusive formation of C_3-symmetrical triple-stranded helicates with comparable geometries (Table 2).

The paramagnetic complexes $[LnCo(L^4)_3]^{6+}$ (Ln = Ce–Eu, Tm and Yb) display sufficiently short electronic relaxation times to allow a dependable assignment of all the NMR signals using well-resolved two-dimensional {^1H–^1H}-COSY and {^1H–^1H}-NOESY spectra, but the large magnetic moments of Ln = Tb–Er prevent the detection of short range NOE effects and the associated NMR spectra are assigned according to a well-established iterative process in which F_i and G_i terms

‡ The detailed description of the complexation properties of $[LnCo(L^4)_3]^{6+}$ will be published elsewhere.

Table 2 ^{1}H NMR shifts (with respect to $SiMe_4$) of $[LnCo(L^4)_3]^{6+}$ in CD_3CN at 298 K

Bidentate binding unit

Compound	Me^1	Me^2	H^1	H^2	H^3	H^4	H^5	H^6
$[LaCo(L^4)_3]^{6+}$	2.25	4.44	6.97	8.15	8.48	7.71	7.23	4.44
$[YCo(L^4)_3]^{6+}$	2.25	4.45	6.97	8.15	8.48	7.76	7.29	4.37
$[LuCo(L^4)_3]^{6+}$	2.24	4.45	6.97	8.15	8.48	7.76	7.29	4.34
$[CeCo(L^4)_3]^{6+}$	1.99	4.02	6.49	7.89	8.08	7.26	6.84	2.42
$[PrCo(L^4)_3]^{6+}$	1.87	3.78	6.19	7.72	7.83	6.94	6.54	1.20
$[NdCo(L^4)_3]^{6+}$	2.06	4.13	6.6	7.96	8.18	7.37	6.92	2.99
$[SmCo(L^4)_3]^{6+}$	2.20	4.37	6.86	7.95	8.11	7.65	7.19	4.46
$[EuCo(L^4)_3]^{6+}$	2.46	4.78	7.32	8.39	8.81	8.15	7.64	6.04
$[TbCo(L^4)_3]^{6+}$	−0.46	−0.19	1.95	5.17	4.04	2.34	2.94	−17.62
$[DyCo(L^4)_3]^{6+}$	−0.53	−0.65	0.04	4.94	3.70	1.80	1.70	−19.20
$[TmCo(L^4)_3]^{6+}$	3.21	6.15	8.76	9.23	10.07	9.92	9.35	12.14
$[YbCo(L^4)_3]^{6+}$	2.65	5.13	7.67	8.59	9.11	8.62	8.13	7.50

Tridentate binding unit

Compound	Me^3	H^9	H^{10}	H^{11}	H^{12}	H^{13}	H^{14}	Me^4	Me^5	H^7	H^8
$[LaCo(L^4)_3]^{6+}$	4.41	5.78	7.15	7.69	8.55	8.31	7.80	0.91	0.73	3.75	3.55
$[YCo(L^4)_3]^{6+}$	4.45	5.42	7.10	7.66	8.63	8.29	7.83	1.01	0.68	3.75	3.60
$[LuCo(L^4)_3]^{6+}$	4.44	5.31	7.09	7.66	8.64	8.28	7.83	1.03	0.66	3.74	3.57
$[CeCo(L^4)_3]^{6+}$	5.35	−0.50	6.67	7.88	10.96	9.97	8.92	−1.17	1.22	3.12	3.12
$[PrCo(L^4)_3]^{6+}$	6.05	−4.50	6.41	8.26	12.80	10.95	9.83	−2.67	1.72	2.78	2.76
$[NdCo(L^4)_3]^{6+}$	5.07	1.48	6.79	8.38	11.15	9.77	9.29	−0.77	1.36	3.30	3.18
$[SmCo(L^4)_3]^{6+}$	4.62	4.05	7.04	7.63	8.89	8.50	8.41	0.34	1.03	3.61	3.53
$[EuCo(L^4)_3]^{6+}$	3.84	9.92	7.50	6.34	4.77	6.42	5.50	2.46	0.42	4.24	4.10
$[TbCo(L^4)_3]^{6+}$	17.07	−68.0	1.95	4.95	28.25	21.05	16.00	−24.1	4.70	−9.02	−2.71
$[DyCo(L^4)_3]^{6+}$	18.80	−76.0	1.55	6.10	31.20	22.70	18.00	−28.7	7.11	−7.52	−2.62
$[TmCo(L^4)_3]^{6+}$	0.80	30.0	8.40	6.53	−0.95	1.24	2.77	9.17	−1.10	5.97	5.12
$[YbCo(L^4)_3]^{6+}$	2.85	15.40	7.59	7.25	5.13	6.19	6.25	4.42	−0.10	4.63	4.18

extracted from the isostructural series are used to calculate predicted spectra of Ln = Tb–Er according to eqn. (2) which are then compared with experimental data.[6,9,27] Mathematical treatment of the paramagnetic shifts given in Table 2 according to eqns. (4) and (5) for $[LnCo(L^4)_3]^{6+}$ (Ln = Ce–Eu) systematically produces linear plots in agreement with the existence of an isostructural series (Fig. 6).‡ The separation of contact and pseudo-contact contributions according to eqn. (2) is straightforward and allows the prediction of ^{1}H NMR chemical shifts for Tb–Yb which match the experimental spectra only for Tb and Dy (Fig. 6). We conclude that smaller metal ions might belong to a second isostructural series. As mentioned above, only Tm and Yb display sufficiently well-resolved NMR spectra to allow a reliable assignment of the signals to protons $H^{1–14}$. Their subsequent location in the plots obtained from eqns. (4), and (5) indeed shows a significant mismatch with the first isostructural series (Fig. 6).

If we consider Yb and Tm as the members of a second series, a new set of contact and pseudo-contact terms can be generated from eqn. (2), which allows new predictions for the spectra of $[LnCo(L^4)_3]^{6+}$ (Ln = Ho, Er). However, experimental data for these complexes do not match these predictions so that *at least three different structures* for $[LnCo(L^4)_3]^{6+}$ are predicted (Ln = Ce–Dy; Ho–Er; Tm–Yb). Considering the similar crystal structures found for La and Lu (Fig. 5) and the rigidity of these assemblies,[6,7] this hypothesis is however counter-intuitive and we suspect that variation of the crystal-field parameter for small Ln^{III} ions is responsible for this unusual behaviour. Application of the crystal-field parameter independent method [eqn. (8)] for each pair of protons (H^i/H^k, $i \neq k$) in $[LnCo(L^4)_3]^{6+}$ indeed results in straight lines for Ce–Dy, Tm and Yb, in agreement with a single geometrical arrangement of the ligands around the metal ions (Fig. 7).

Table 3 collects the experimental slopes and intercepts together with their expected values calculated from the C_3-averaged X-ray crystal structure of $[LaCo(L^4)_3](ClO_4)_{5.5}(OH)_{0.5}$

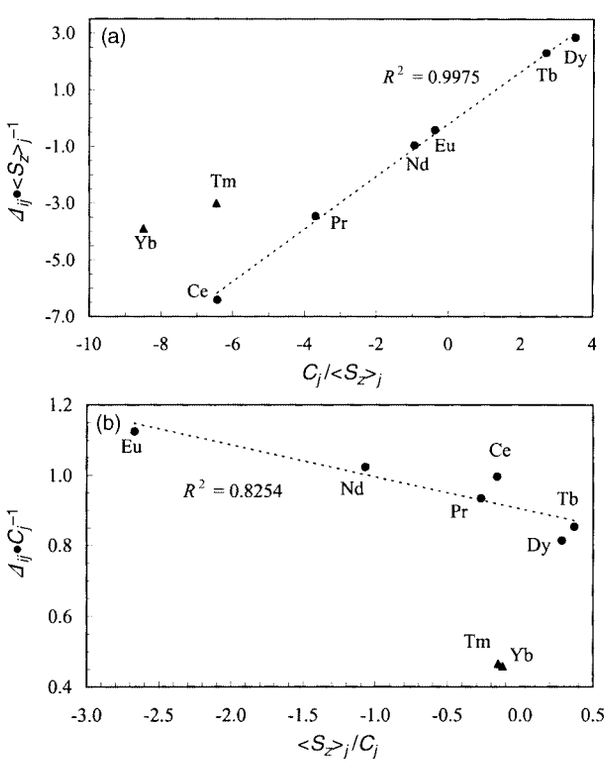

Fig. 6 Plots of (a) $\Delta_{ij}\cdot\langle S_z\rangle_j^{-1}$ *vs.* $C_j\cdot\langle S_z\rangle_j^{-1}$ [eqn. (4)] and (b) $\Delta_{ij}\cdot C_j^{-1}$ *vs.* $\langle S_z\rangle_j\cdot C_j^{-1}$ [eqn. (5)] for H^9 in $[LnCo(L^4)_3]^{6+}$ (acetonitrile, 298 K).

and the F_i and F_k values obtained according to eqn. (2) for the isostructural series Ce–Dy.[7]‡ The calculated and experimental R_{ik} values are in good agreement except for pairs involving H^{11} whose θ_i angle ($\theta_{H^{11}} = 53.8°$ in the crystal structure) is close to the magic angle (54.7°) for which the geometrical term $1 - 3$

Table 3 Minimal set of geometric ratio $R_{ik} = G_i \cdot G_k^{-1}$ obtained from plots of $\Delta_{ij} \cdot \langle S_z \rangle_j^{-1}$ *vs.* $\Delta_{kj} \cdot \langle S_z \rangle_j^{-1}$ according to eqn. (8) for $[LnCo(L^4)_3]^{6+}$ (CD_3CN, 298 K)[a]

	H^1–H^2	H^1–H^3	H^1–H^4	H^1–H^5	H^1–H^6	H^1–H^9
R_{ik}[b]	1.83(6)	1.22(3)	1.00(5)	1.10(8)	0.244(7)	0.076(2)
R_{ik} (cryst.)[c]	1.648	1.115	1.243	2.013	0.232	1.107
	H^1–H^{10}	H^1–H^{11}	H^1–H^{12}	H^1–H^{13}	H^1–H^{14}	
R_{ik}[b]	1.07(6)	−4.6(7)	−0.22(1)	−0.33(2)	−0.48(2)	
R_{ik} (cryst.)[c]	1.376	9.736	−0.228	−0.417	−0.500	

[a] A complete set of R_{ik} data generated according to $R_{ik} = R_{ij} \cdot R_{jk}$ is given in the supporting information together with the experimental and calculated intercepts $F_i - R_{ik} \cdot F_k$ (Table S2). [b] Values for the isostructural series (Ln = Ce–Yb, Sm has been removed because of its faint paramagnetic induced shift). [c] Calculated from the crystal structure of $[LaCo(L^4)_3](ClO_4)_{5.5}(OH)_{0.5}$ after averaging to C_3 symmetry.[7]

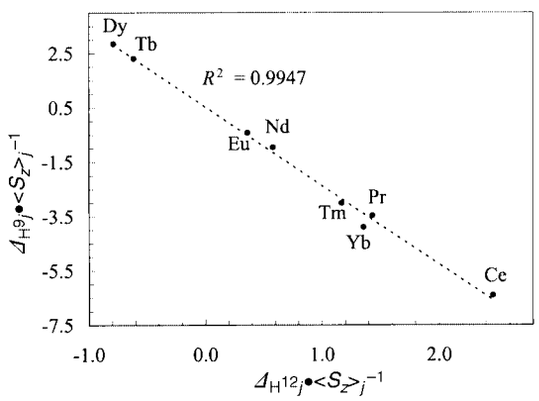

Fig. 7 Plot of $\Delta_{ij} \cdot \langle S_z \rangle_j^{-1}$ *vs.* $\Delta_{kj} \cdot \langle S_z \rangle_j^{-1}$ according to eqn. (8) for H^9–H^{12} in $[LnCo(L^4)_3]^{6+}$ (acetonitrile, 298 K).

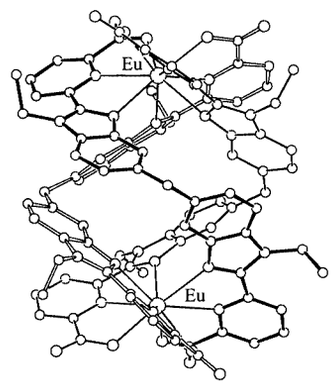

Fig. 8 ORTEP[24] view of $[Eu_2(L^5 - 2H)_3]$ perpendicular to the pseudo-C_3 axis in the crystal structure of $[Eu_2(L^5 - 2H)_3] \cdot 20.5H_2O$.[9]

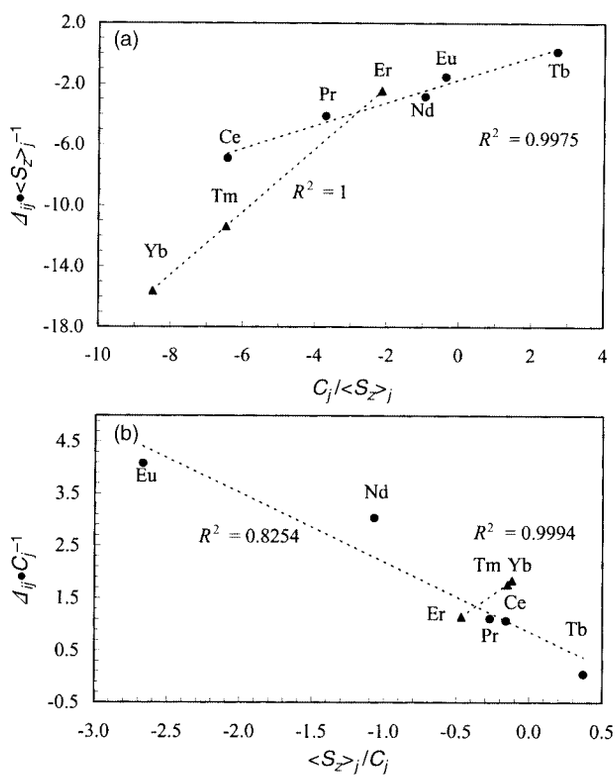

Fig. 9 Plots of (a) $\Delta_{ij} \cdot \langle S_z \rangle^{-1}$ *vs.* $C_j \cdot \langle S_z \rangle_j^{-1}$ and (b) $\Delta_{ij} \cdot C_j^{-1}$ *vs.* $\langle S_z \rangle_j \cdot C_j^{-1}$ for $H^{4'}$ in $[Ln_2(L^5 - 2H)_3]$ (water, 298 K).

$\cos^2(\theta_i) \approx 0$. The pairs containing H^{11} have thus been excluded for the calculation of the agreement factor [eqn. (10)] which amounts to $AF_{slope} = 0.18$ (Ce–Yb) and points to a satisfying match between the solid state structure of $[LaCo(L^4)_3]^{6+}$ and the solution structure of $[LnCo(L^4)_3]^{6+}$ for the complete lanthanide series. The worse agreements between solution and solid state structures correspond to pairs involving H^5 since $\theta_{H^5} = 49.7°$ in the crystal structure, a value which is still close to the magic angle. We conclude that (i) the breaks obtained with eqns. (4) and (5) for small Ln^{III} result from changes in the crystal-field parameter as previously suggested for related observations with C_4-symmetrical macrocyclic lanthanide complexes,[15] (ii) no significant geometrical changes occur along the lanthanide series in agreement with the similar crystal structures found for La and Lu and (iii) the rigidity of the dimetallic triple helical edifice ensures similar geometrical arrangements in the solid state and in solution.

Homodimetallic f–f triple helical complexes: $[Ln_2(L^5 - 2H)_3]$

Previous NMR investigations strongly suggest that the diamagnetic triple-stranded helicates $[Ln_2(L^5 - 2H)_3]$ in D_2O (Ln = La, Y, Lu) adopt a kinetically inert D_3-symmetrical triple helical structure similar to that found in the crystal structure of $[Eu_2(L^5 - 2H)_3]$ (Fig. 8).[9] However, an analysis of the paramagnetic NMR shifts of H^i (i = 3–5, 4′, 6′, 7′), b-CH_2 and Me according to eqns. (4) and (5) shows systematic breaks between large (Ce–Tb) and small (Er–Yb) Ln^{III} ions as previously described for $[Ln(L^2)_3]^{3+}$ (Fig. 9),[9] thus suggesting a possible geometrical change along the series.

Since the residual paramagnetic dipolar contributions to the NMR shifts result from two paramagnetic centres, the separation of contact and pseudo-contact contributions within each isostructural series following the method of Reilley and coworkers[13] requires the replacement of eqn. (2) by eqn. (11) where

$$\Delta_{ij} = \delta_{ij} - \delta_i^{dia} = \delta_{ij}^{c} + \delta_{ij}^{pc} = F_i \cdot \langle S_z \rangle_j + (G_i^1 + G_i^2) \cdot \{A_2^0 \cdot \langle r^2 \rangle\} \cdot \frac{C_j}{T^2} \quad (11)$$

the three following hypotheses are satisfied:[9] (1) no magnetic coupling between the two Ln^{III} can be detected within the temperature range of the NMR measurements,[28] (2) the contact contributions are limited to through-bond Fermi interactions originating from a single paramagnetic metallic centre and (3) the z-axis of the magnetic susceptibility tensor coincides with the intermetallic axis. We have demonstrated that these criteria are fulfilled for the C_3-symmetrical helicates $[Ln_2(L^5 - 2H)_3]$[9] and eqn. (11) gives contact terms (F_i) and global pseudo-

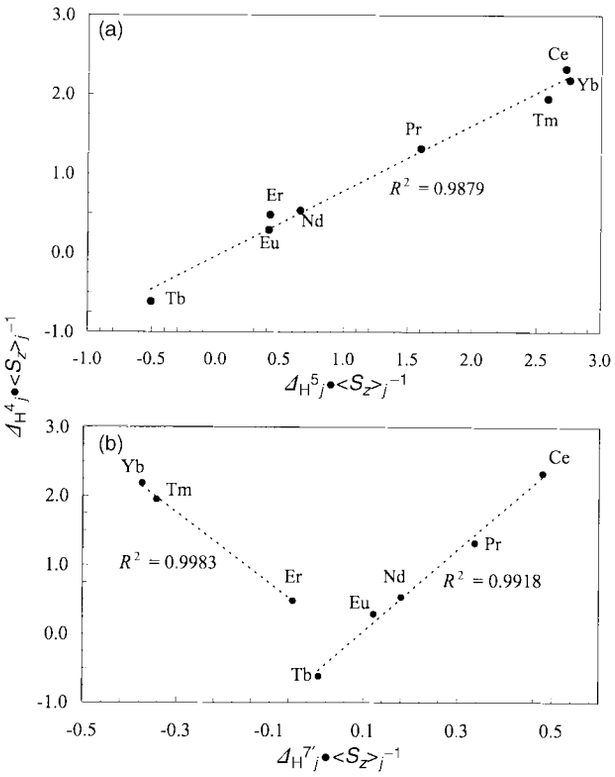

Fig. 10 Plots of $\Delta_{ij} \cdot \langle S_z \rangle_j^{-1}$ *vs.* $\Delta_{kj} \cdot \langle S_z \rangle_j^{-1}$ according to eqn. (13) for (a) H^4–H^5 and (b) H^4–$H^{7'}$ in $[Ln_2(L^5 - 2H)_3]$ (water, 298 K).

contact terms ($G_i^{global} = G_i^1 + G_i^2$) for each nucleus which can be analysed according to eqn. (12) provided that r_i^n and θ_i^n are the internal axial co-ordinates of nucleus i with respect to the ligand field axis of site n (Fig. 1).[9]

$$(G_i^1 + G_i^2) = \sum_{n=1}^{2} \left(\frac{1 - 3\cos^2 \theta_i^n}{(r_i^n)^3} \right) \quad (12)$$

The influence of the crystal-field parameter can be removed as previously established for monometallic complexes:

$$\frac{\Delta_{ij}}{\langle S_z \rangle_j} = \left[F_i - F_k \cdot \frac{(G_i^1 + G_i^2)}{(G_k^1 + G_k^2)} \right] + \frac{(G_i^1 + G_i^2)}{(G_k^1 + G_k^2)} \cdot \frac{\Delta_{kj}}{\langle S_z \rangle_j} \quad (13)$$

$$R_{ik} = \frac{(G_i^1 + G_i^2)}{(G_k^1 + G_k^2)} = \left[\frac{(r_i^2)^3 \cdot (1 - 3\cos^2 \theta_i^1) + (r_i^1)^3 \cdot (1 - 3\cos^2 \theta_i^2)}{(r_k^2)^3 \cdot (1 - 3\cos^2 \theta_k^1) + (r_k^1)^3 \cdot (1 - 3\cos^2 \theta_k^2)} \right] \cdot \left[\frac{(r_k^1)^3 \cdot (r_k^2)^3}{(r_i^1)^3 \cdot (r_i^2)^3} \right] \quad (14)$$

Plots of $\Delta_{ij}/\langle S_z \rangle_j$ *vs.* $\Delta_{kj}/\langle S_z \rangle_j$ according to eqn. (13) for the various possible pairs of paramagnetic NMR shifts arising from $H^{3\text{–}5,4',6',7'}$, b-CH_2 and Me in $[Ln_2(L^5 - 2H)_3]$ show three different behaviours depending on the protons involved (Fig. 10). First, no obvious correlation is observed for pairs involving $H^{6'}$ which can be explained by the peculiar location of this proton in the triple-stranded helicate. According to the D_3-averaged crystal-structure of $[Eu_2(L^5 - 2H)_3]$, we calculate axial co-ordinates of $\theta_{H^{6'}}^1 = 54.1°$ and $\theta_{H^{6'}}^2 = 55.0°$ which are both close to the magic angle (54.7°) and lead to a dramatic sensitivity to faint structural changes along the lanthanide series as previously discussed for H^{11} in $[LnCo(L^4)_3]^{6+}$ and C^4 in $[Eu(L^2)_3]^{3+}$. Nevertheless, this observation points to possible minor geometrical changes from one lanthanide to the other,

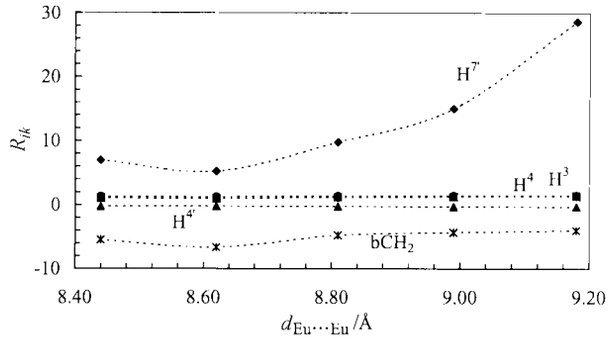

Fig. 11 Calculated R_{ik} factors for pairs H^5–H^k (k = 3, 4, 4′, 7′) and H^5–b-CH_2 in the crystal structure of $[Ln_2(L^5 - 2H)_3]$ (intermetallic distance d varies from 8.4 to 9.2 Å, see Table 4).

but we cannot conclude that a significant structural variation occurs along the series and the pairs involving $H^{6'}$ have been neglected in the final statistical analysis. Second, pairs involving protons $H^{3\text{–}5,4'}$, b-CH_2 and Me display a single straight line for the complete lanthanide series (Ce–Yb, Fig. 10a) as similarly observed for $[LnCo(L^4)_3]^{6+}$ which indicates that: (i) no significant structural variation occurs along the complete lanthanide series, (ii) changes in the crystal-field parameters are responsible for the breaks observed between Tb and Er (Fig. 9) and (iii) similar hyperfine coupling constants hold for all studied lanthanide ions, in agreement with a single structure along the series.

Finally, related plots according to eqn. (13) involving $H^{7'}$ clearly exhibit two straight lines, one for the large (Ce, Tb) and one for the small (Er, Yb) Ln^{III} ions with an abrupt transition between them (Fig. 10b). This behaviour contrasts with that observed for $H^{3\text{–}5,4'}$, b-CH_2 and Me and apparently leads to opposite conclusions in which two different structural arrangements should be invoked. However, both metallic centres significantly contribute to the paramagnetic shift of $H^{7'}$ ($G_{H^{7'}}^1/G_{H^{7'}}^2 = 0.58$) and the $\theta_{H^{7'}}^i$ (i = 1, 2) are distributed on both sides of the magic angles (49.1° and 63.0° according to the crystal structure for Eu). We thus suspect that the paramagnetic shift of $H^{7'}$ is particularly sensitive to minor structural variations as a result of its peculiar geometrical location and, in order to support this hypothesis, we have calculated the expected R_{ik} factor for pairs involving this proton (H^i–$H^{7'}$) when the Eu · · · Eu distance is increased by stepwise increments of ≈0.2 Å from 8.4 Å to 9.2 Å and the ligands are fixed in their conformations found in the crystal structure of $[Eu_2(L^5 - 2H)_3]$ for which Eu · · · Eu = 8.81 Å [Table 4; for pairs involving $H^{7'}$, no R_{ik} factors are reported for the complexes in solution because two different straight lines are observed (Fig. 10b)].

The R_{ik} values found in solution are in good agreement with those calculated from the averaged D_3-symmetrical crystal structure leading to an agreement factor $AF_{slope} = 0.17$ and to the conclusion that the crystal structure of $[Eu_2(L^5 - 2H)_3]$ is a satisfying model for the complexes in solution along the complete lanthanide series. The simulated R_{ik} obtained by varying the intermetallic distance from 8.4 to 9.2 Å display small variations for $H^{3\text{–}5,4'}$, b-CH_2 and Me while pairs involving $H^{7'}$ display drastic changes which confirms their extreme sensitivity to minor structural changes (Table 4, Fig. 11). We conclude that this nucleus is sensitive to faint geometrical variations in the complex which are not detected by other protons, in agreement with the existence of a single isostructural series for $[Ln_2(L^5 - 2H)_3]$ (Ln = Ce–Yb) modulated by minor structural changes associated with the standard lanthanide contraction. The X-ray crystal structure of $[Yb_2(L^5 - 2H)_3]$ substantiates this reasoning since the triple helical structure is very similar to those determined for Eu and Tb,[9] except for a larger intermetallic distance (Yb · · · Yb = 9.11 Å) reflecting a lengthening of the helix and a tighter co-ordination of the carboxylate groups.

Table 4 Minimal set of geometric ratio $R_{ik} = (G_i^1 + G_i^2)\cdot(G_k^1 + G_k^2)^{-1}$ obtained from plots of $\Delta_{ij}\cdot\langle S_z\rangle_j^{-1}$ *vs.* $\Delta_{kj}\cdot\langle S_z\rangle_j^{-1}$ according to eqn. (13) for $[Ln_2(L^5 - 2H)_3]$ (D_2O, 298 K)[a]

R_{ik}	b-CH_2–H^3	b-CH_2–H^4	b-CH_2–H^5	b-CH_2–$H^{4'}$	b-CH_2–$H^{6'}$	b-CH_2–$H^{7'}$
(Ce–Yb)[b]	−0.32(1)	−0.33(1)	−0.27(1)	0.049(2)	2.3(4)	[e]
d = 8.81 Å[c]	−0.250	−0.296	−0.210	0.051	4.433	−2.048
d = 8.44 Å[d]	−0.200	−0.246	−0.183	0.042	13.175	−1.273
d = 8.62 Å[d]	−0.150	−0.193	−0.151	0.032	−5.977	−0.788
d = 8.99 Å[d]	−0.303	−0.344	−0.233	0.059	3.053	−3.500
d = 9.18 Å[d]	−0.389	−0.389	−0.253	0.068	2.488	−7.241

[a] A complete set of R_{ik} data generated according to $R_{ik} = R_{ij}\cdot R_{jk}$ is given in the supporting information (Table S3). [b] Sm has been removed because of its faint paramagnetism.[9] [c] Calculated from the crystal structure of $[Eu_2(L^5 - 2H)_3]$ after averaging to D_3 symmetry.[9] [d] Calculated from the crystal structure of $[Eu_2(L^5 - 2H)_3]$ with a fixed intermetallic distance and after averaging to D_3 symmetry (see text). [e] No R_{ik} values are obtained (see text).

Conclusion

These examples clearly establish that the model-independent method described by eqn. (2) (monometallic) and eqn. (11) (bimetallic) for dissecting contact and pseudo-contact contributions introduces some limitations in the interpretation of solution structures because the origin of breaks in the linear plots of eqns. (4) and (5) can be the result of either: (i) the regular contraction of the lanthanide ionic radii with increasing atomic numbers,[12] (ii) an abrupt geometrical change along the series or (iii) a significant variation of the crystal-field parameter from one lanthanide to the other.[15] Our previous studies of the triple helical lanthanide complexes[4,6–9] suffered from these limitations leading to only partial conclusions regarding their solution structures. The application of the crystal-field independent technique according to its recent formulation by Geraldes and co-workers [eqn. (8)][17] allows a reliable investigation of geometrical and/or electronic changes occurring along the lanthanide series for complexes possessing a single paramagnetic centre.

For $[Ln(L^2)_3]^{3+}$ in acetonitrile, the different structures adopted by large (Ce–Tb) and small (Er–Yb) lanthanides previously suggested on the basis of (i) variable temperature NMR data, (ii) breaks in plots according to eqns. (4) and (5) and (iii) X-ray crystal structures[4] is unambiguously confirmed by the systematic observation of two different linear plots for eqn. (8). The complexes with Ln = Ce–Tb are labile on the NMR time scale at room temperature and indeed exhibit dynamically-averaged D_{3h}-symmetry resulting from the fast interconversion between the helical enantiomers while blocked triple-helical structures possessing D_3-symmetry characterise the related complexes with Ln = Er–Yb. An extension of this approach to the kinetically inert and rigid heterodimetallic triple-stranded helicate $[LnCo(L^4)_3]^{6+}$ successfully establishes that a single isostructural series is observed for the complete lanthanide series. Significant variations in the crystal-field parameters for the small Ln^{III} are responsible for the failure of eqns. (4) and (5) to rationalise the structures of these complexes in solution.

Recently, a detailed spectroscopic investigation of the electronic state structure of $Na_3[Ln(L^1 - 2H)_3]$ in the solid state (Ln = Nd, Sm, Eu, Gd, Tb, Dy, Ho, Er)[29] has shown that the crystal-field interaction strength (S_{cf}) significantly varies along the lanthanide series with values in the range 341–433 [mean 390(50)] for Nd–Tb and 279–297 [mean 290(30)] for heavy lanthanide ions, pointing to significantly smaller interactions when the 4f orbitals are contracted.[29] It is worth noting that the variation of the crystal-field strength significantly deviates from the expected smooth decrease associated with the regular contraction of 4f orbitals along the lanthanide series as suggested by (i) the unpredictable crystal-field parameters found for macrocyclic complexes with Ln = Tb–Yb ($146 \leq \{A_2^0\cdot\langle r^2\rangle\} \leq 358$,[15] the smallest value corresponding to Yb and the largest to the neighbouring element Tm) and (ii) a previous report claiming that Tm^{III} has the largest crystal-field splitting among the Ln series.[30]

The related eqns. (11)–(14) have proved to be well adapted for the structural investigation of bimetallic complexes in which large Ln···Ln distances prevent significant magnetic exchange, as proven by the analysis of the homodimetallic triple helical $[Ln_2(L^5 - 2H)_3]$ assemblies. The use of the crystal-field independent eqn. (13) unambiguously establishes the existence of a single isostructural series in acetonitrile which is in line with the similar crystal structures found for Ln = Eu, Tb and Yb in the solid state. Again, the breaks observed with the classical method [eqn. (11)][9] do not reflect geometrical changes along the lanthanide series, but crystal-field variations. We note however that the interpretation may be sometimes complicated by the peculiar sensitivity of specific protons to minor structural changes.

In conclusion, the usual assumption that the crystal-field parameter is essentially constant along the complete lanthanide series is systematically wrong for the triple-helical complexes we have studied and no structural predictions can be drawn from the model-independent method [eqns. (2) and (11)]. The crystal-field independent method [eqns. (8) and (13)] significantly improves the quality of the structural investigations which opens new perspectives for the characterisation of sophisticated polymetallic lanthanide complexes in solution and for the interpretation of NMR spectra of complexes incorporating Tb–Er and for which NOE's cannot be recorded.

Experimental

The complexes $[Ln(L^2)_3](TfO)_3$,[4] $[LnCo(L^4)_3](ClO_4)_6$,[7,‡] and $[Ln_2(L^5 - 2H)_3]$[9] were prepared according to literature procedures and dissolved in CD_3CN or D_2O. ^1H NMR spectra were recorded at 25 °C on a Broadband Varian Gemini 300 spectrometer and a Bruker AVANCE DRX400 spectrometer. Chemical shifts are given in ppm with respect to internal TMS.

Acknowledgements

We are grateful to Dr M. Elhabiri and Dr F. Renaud for sending electronic files containing the chemical shifts of $[Ln(L^2)_3]^{3+}$[4] and $[Ln_2(L^5 - 2H)_3]$.[9] This work is supported through grants from the Swiss National Science Foundation.

References

1 For reviews, see C. Piguet and J.-C. G. Bünzli, *Chem. Soc. Rev.*, 1999, **28**, 347. C. Piguet, *Chimia*, 1996, **50**, 144. C. Piguet, C. Edder, H. Nozary, F. Renaud, S. Rigault and J.-C. G. Bünzli, *J. Alloys Comp.*, in press, J.-C. G. Bünzli, N. André, M. Elhabiri, G. Müller and C. Piguet, *J. Alloys Comp.*, in press.

2 R. D. Champman, R. T. Loda, J. P. Riehl and R. W. Schwartz, *Inorg. Chem.*, 1984, **23**, 1652. C. Mallet, R. P. Thummel and C. Hery, *Inorg. Chim. Acta*, 1993, **210**, 223.

3 I. Grenthe, *J. Am. Chem. Soc.*, 1961, **83**, 360. J. M. Harrowfield, Y. Kim, B. W. Skelton and A. H. White, *Aust. J. Chem.*, 1995, **48**, 807 and references therein.

4 F. Renaud, C. Piguet, G. Bernardinelli, J.-C. G. Bünzli and G. Hopfgartner, *Chem. Eur. J.*, 1997, **3**, 1646.

5 S. Petoud, J.-C. G. Bünzli, F. Renaud, C. Piguet, K. J. Schenk and G. Hopfgartner, *Inorg. Chem.*, 1997, **36**, 5750. C. Piguet, J.-C. G. Bünzli, G. Bernardinelli, C. G. Bochet and P. Froidevaux, *J. Chem.*

Soc., *Dalton Trans.*, 1995, 83. C. Piguet, A. F. Williams, G. Bernardinelli and J.-C. G. Bünzli, *Inorg. Chem.*, 1993, **32**, 4139.
6 C. Edder, C. Piguet, J.-C. G. Bünzli and G. Hopfgartner, *J. Chem. Soc.*, *Dalton Trans.*, 1997, 4757. C. Piguet, J.-C. G. Bünzli, G. Bernardinelli, G. Hopfgartner, S. Petoud and O. Schaad, *J. Am. Chem. Soc.*, 1996, **118**, 6681. J.-P. Costes, F. Dahan, A. Dupuis, S. Lagrave and J.-P. Laurent, *Inorg. Chem.*, 1998, **37**, 153. J.-P. Costes, A. Dupuis and J.-P. Laurent, *Inorg. Chim. Acta*, 1998, **268**, 125.
7 S. Rigault, C. Piguet, G. Bernardinelli and G. Hopfgartner, *Angew. Chem.*, *Int. Ed.*, 1998, **37**, 169.
8 C. Piguet, J.-C. G. Bünzli, G. Bernardinelli, G. Hopfgartner and A. F. Williams, *J. Am.*, *Chem. Soc*., 1993, **115**, 8197. N. Martin, J.-C. G. Bünzli, V. McKee, C. Piguet and G. Hopfgartner, *Inorg. Chem.*, 1998, **37**, 577.
9 M. Elhabiri, R. Scopelliti, J.-C. G. Bünzli and C. Piguet, *Chem. Commun.*, 1998, 2347. M. Elhabiri, R. Scopelliti, J.-C. G. Bünzli and C. Piguet, *J. Am. Chem. Soc.*, 1999, **121**, 10747.
10 J. M. Briggs, G. P. Moss, E. W. Randal and K. D. Sales, *J. Chem. Soc.*, *Chem. Commun.*, 1972, 1180.
11 For recent reviews, see S. P. Babailov and Y. G. Kreiger, *J. Struct. Chem.*, 1998, **39**, 580. I. Bertini and C. Luchinat, *Coord. Chem. Rev.*, 1996, **150**, 1.
12 J. A. Peters, J. Huskens and D. J. Raber, *Prog. NMR Spectrosc.*, 1996, **28**, 382. J. A. Peters, *J. Magn. Reson.*, 1986, **68**, 240.
13 J. F. Desreux and C. N. Reilley, *J. Am. Chem. Soc.*, 1976, **98**, 2105. C. N. Reilley, B. W. Good and J. F. Desreux, *Anal. Chem.*, 1975, **47**, 2110. C. N. Reilley, B. W. Good and R. D. Allendoerfer, *Anal. Chem.*, 1976, **48**, 1446.
14 M. D. Kemple, B. D. Ray, K. B. Lipkowitz, F. G. Prendergast and B. D. N. Rao, *J. Am. Chem. Soc*., 1988, **110**, 8275.
15 J. Ren and A. D. Sherry, *J. Magn. Reson.*, 1996, **B111**, 178.
16 J. Reuben, *J. Magn. Reson.*, 1982, **50**, 233.
17 C. Platas, F. Avecilla, A. de Blas, C. F. G. C. Geraldes, T. Rodrigues-Blas, H. Adams and J. Mahia, *Inorg. Chem.*, 1999, **38**, 3190.
18 R. M. Golding and M. P. Halton, *Aust. J. Chem.*, 1972, **25**, 2577.
19 B. J. Bleaney, *J. Magn. Reson.*, 1972, **8**, 91. J. Reuben and G. A. Elgavish, *J. Magn. Reson.*, 1980, **39**, 421.
20 P. Caravan, P. Mehrkhodavandi and C. Orvig, *Inorg. Chem.*, 1997, **36**, 1316.
21 W. C. Dickinson, *Phys. Rev.*, 1959, **81**, 717. C. Piguet, *J. Chem. Educ.*, 1997, **74**, 815 and references therein.
22 For a review, see A. D. Sherry and C. F. G. C. Geraldes, in *Lanthanide Probes in Life*, *Chemical and Earth Sciences*, eds. J.-C. G. Bünzli and G. R. Choppin, Elsevier, Amsterdam, 1989, ch. 4.
23 C. F. G. C. Geraldes, A. D. Sherry and G. E. Kiefer, *J. Magn. Reson.*, 1992, **97**, 290.
24 C. K. Johnson, ORTEP II, Report ORNL-5138, Oak Ridge National Laboratory, Oak Ridge, TN, 1976.
25 C. Piguet, G. Bernardinelli and G. Hopfgartner, *Chem. Rev.*, 1997, **97**, 2005.
26 M. Meyer, B. Kersting, R. E. Powers and K. N. Raymond, *Inorg. Chem.*, 1997, **36**, 5179. L. J. Charbonnière, A. F. Williams, U. Frey, A. E. Merbach, P. Kamalaprija and O. Schaad, *J. Am. Chem. Soc.*, 1997, **119**, 2488. M. Albrecht and M. Schneider, *Chem. Commun.*, 1997, 137.
27 J. H. Forsberg, R. M. Delaney, Q. Zhao, G. Harakas and R. Chandran, *Inorg. Chem.*, 1995, **34**, 3705.
28 J.-P. Costes, F. Dahan, A. Dupuis, S. Lagrave and J.-P. Laurent, *Inorg. Chem.*, 1998, **37**, 153.
29 T. A. Hopkins, D. H. Metcalf and R. S. Richardson, *Inorg. Chem.*, 1998, **37**, 1401.
30 B. M. Alsaadi, R. J. C. Rossotti and R. J. P. Williams, *J. Chem. Soc.*, *Dalton Trans.*, 1980, 2151.